Variational Quantum Gibbs State Preparation with a Truncated Taylor Series

Youle Wang,[1,2] Guangxi Li,[1,2] and Xin Wang[1,*]

[1] *Institute for Quantum Computing, Baidu Research, Beijing 100193, China*

[2] *Centre for Quantum Software and Information, University of Technology, Sydney, New South Wales 2007, Australia*

(Received 31 March 2021; revised 28 June 2021; accepted 12 October 2021; published 18 November 2021)

The preparation of a quantum Gibbs state is an essential part of quantum computation and has wide-ranging applications in various areas, including quantum simulation, quantum optimization, and quantum machine learning. In this paper, we propose variational hybrid quantum-classical algorithms for quantum Gibbs state preparation. We first utilize a truncated Taylor series to evaluate the free energy and choose the truncated free energy as the loss function. Our protocol then trains the parameterized quantum circuits to learn the desired quantum Gibbs state. Notably, this algorithm can be implemented on near-term quantum computers equipped with parameterized quantum circuits. By performing numerical experiments, we show that shallow parameterized circuits with only one additional qubit can be trained to prepare the Ising chain and spin chain Gibbs states with a fidelity higher than 95%. In particular, for the Ising chain model, we find that a simplified circuit ansatz with only one parameter and one additional qubit can be trained to realize a 99% fidelity in Gibbs state preparation at inverse temperatures larger than 2.

DOI: 10.1103/PhysRevApplied.16.054035

I. INTRODUCTION

Quantum state preparation is an integral part of quantum computation. In the near future, quantum computers will become quantum state preparation factories for various tasks. One central task in quantum state preparation is to prepare the quantum Gibbs or thermal state of a given Hamiltonian. The reason is that quantum Gibbs states can not only be used to study many-body physics, but can also be applied to quantum simulation [1], quantum machine learning [2,3], and quantum optimization [4]. In particular, sampling from well-prepared Gibbs states of Hamiltonians can be applied in solving combinatorial optimization problems [4], solving semidefinite programs [5], and training quantum Boltzmann machines [6].

The preparation of the desired initial state is a difficult problem in general. It is well known that finding ground states of Hamiltonians is QMA hard [7]. Gibbs state preparation at arbitrary low temperature could be as hard as finding the ground state [8]. There are various methods to do this using classical [9–13] or quantum computers. Notably, these methods use quantum computing techniques, including quantum rejection sampling [14], quantum walk [15], dynamics simulation [16–18], dimension reduction [19]. Although in the worst case, the costs that these methods require could be exponential in expectation, they can be efficient when certain conditions are satisfied, such as when the ratios between the partition functions of the infinite temperature states and the Gibbs state are at most polynomially large [10], and the gap of the Markov chain that describes the quantum walk is polynomially small [15,20]. However, these methods require complex quantum subroutines such as quantum phase estimation, which are costly and hard to implement on near-term quantum computers.

The main goal of our work is to prepare quantum Gibbs states using near-term quantum devices. In contrast to the previous works, we aim to reduce the task's quantum resources, such as qubit and gate counts, circuit size. To this end, one feasible scheme is to take advantage of variational quantum algorithms (VQAs) [21], which have recently been gaining popularity with applications in many areas [22–33]. VQAs are a class of hybrid quantum-classical algorithms that involves optimizing a loss function depending on the circuit's parameters, where the loss function is evaluated on quantum devices, and parameter adjustments are outsourced to the classical devices. This strategy succeeds in reducing the resources by using shallow quantum circuits. Several methods based on VQAs have already been proposed [18,34–40] to prepare Gibbs states. For instance, Wu and Hsieh [36] proposed a variational approach by using Rényi entropy estimation [34] and thermofield double states, Yuan *et al.* [39] discussed the application of imaginary time evolution to the Gibbs state using parameterized circuits, and Chowdhury *et al.* [40] proposed an entropy estimation method using tools

*wangxin73@baidu.com

such as quantum amplitude estimation and the linear combination of unitaries.

In this paper, we propose variational quantum algorithms to tackle the problem of Gibbs state preparation on near-term quantum hardware. In general, a Gibbs state of the system's Hamiltonian H at the inverse temperature $\beta = 1/k_B T$ is defined as $\rho_G = e^{-\beta H}/\operatorname{tr}(e^{-\beta H})$, where k_B is the Boltzmann constant and T is the system's temperature. To prepare ρ_G, we utilize the variational principle of the system's free energy [41], which states that the Gibbs state minimizes the free energy. Let the system's state be ρ; then the free energy is given by $\mathcal{F}(\rho) = \operatorname{tr}(H\rho) - \beta^{-1}S(\rho)$, where $S(\rho)$ denotes the von Neumann entropy. Then ρ_G is the global minimum of the functional $\mathcal{F}(\rho)$. In our approach, we use parameterized quantum circuits (PQCs) to prepare quantum states. Particularly, the PQCs are assumed to admit enough expressiveness to prepare the desired Gibbs states or a state very close to it. Throughout the paper, the state prepared via a PQC is denoted by $\rho(\boldsymbol{\theta})$. Using such notation, the variational principle could be formulated as

$$\rho_G \approx \operatorname{argmin}_{\boldsymbol{\theta}} \mathcal{F}[\rho(\boldsymbol{\theta})]. \tag{1}$$

Our goal is to find the optimal parameters that minimize the free energy, given a suitable PQC. Viewed from this point, we could prepare a state very close to the desired state ρ_G.

The main challenge of minimizing the free energy comes from the entropy estimation, which is well known to be difficult [42]. To overcome this challenge, we truncate the Taylor series of the entropy at order K and set the truncated free energy as the loss function in our variational quantum algorithms. Explicitly, the loss function is represented as a linear combination of the system's energy and higher-order state overlaps. The energy and state overlaps are efficiently estimated via certain quantum gadgets, which could be performed on near-term quantum hardware. Hence, our algorithms for Gibbs state preparation are expected to be practical.

We also study the effectiveness of our variational quantum algorithms in Gibbs state preparation. Specifically, we theoretically show that fidelity between the output state of our approach and the target Gibbs state increases as the truncation order K increases. To demonstrate the efficacy of our approach, we focus on the loss function with truncation order 2. We numerically find that using the loss function with order 2 suffices to prepare high-fidelity Gibbs states of several many-body Hamiltonians at selected low temperatures. As shown in the numerical results, the final fidelity could reach at least 95% for the Ising chain and XY spin-$\frac{1}{2}$ chain models, respectively. In particular, the preparation of Ising chain Gibbs states achieves a fidelity above 99%. Besides, we show that our approach applies to prepare Gibbs states at high temperatures. Overall, the numerical results imply that we could prepare high-fidelity Gibbs states of certain many-body Hamiltonians using low-order loss functions, strengthening the feasibility of our approach on near-term quantum hardware.

Our paper is organized as follows. In Sec. II, we describe the main results of this paper, including the variational algorithm for Gibbs state preparation, error analysis, and the analytical gradient of the loss function for optimization. In Sec. III, we numerically demonstrate the effectiveness of our algorithm, especially at lower and higher temperatures, via targeting the Gibbs state preparation of the Ising model and XY spin-$\frac{1}{2}$ model. Then we conclude in Sec. IV. Finally, detailed proofs are provided in Appendix B.

II. MAIN RESULTS

A. Hybrid quantum-classical algorithm for Gibbs state preparation

The Gibbs state for a quantum Hamiltonian H is defined as the density operator

$$\rho = \frac{\exp(-\beta H)}{\operatorname{tr}[\exp(-\beta H)]}. \tag{2}$$

We recall that the free energy of a system described by a density operator ω is given by

$$\mathcal{F}(\omega) = \operatorname{tr}(\omega H) - \beta^{-1}S(\omega), \tag{3}$$

where $\beta = (k_B T)^{-1}$ is the inverse temperature of the system, k_B is the Boltzmann's constant, and $S(\rho) := -\operatorname{tr}\rho\ln\rho$ is the von Neumann entropy of ρ. As the Gibbs state minimizes the free energy of the Hamiltonian H, it holds that

$$\rho = \operatorname{argmin}_{\omega} \mathcal{F}(\omega). \tag{4}$$

Therefore, if we could generate parameterized quantum states $\omega(\boldsymbol{\theta})$ and find a way to measure or estimate the loss function $\operatorname{tr}(\omega H) - k_B T \times S(\omega)$, then one could design variational algorithms via the optimization over $\boldsymbol{\theta}$ [36,40].

Determining the von Neumann entropy of a quantum state on near-term quantum devices is however quite challenging. Existing quantum algorithms for estimating certain entropic quantities [40,43,44] are not suitable for our purpose of using near-term quantum devices since they either have an explicit polynomial dependence on the Hilbert-space dimension of the quantum system or require a certain oracle assumption. Recently, Chowdhury *et al.* [40] proposed a procedure for estimating the von Neumann entropy and free energy that uses tools such as quantum amplitude estimation [45], density matrix exponentiation [46], and techniques for approximating operators by a linear combination of unitaries.

To design a suitable and efficient variational quantum algorithm for near-term quantum devices, we design a loss

function in the similar spirit of free energy. This loss function utilizes the truncated Taylor series and, in particular, can be efficiently estimated on near-term quantum devices. Specifically, the core of our idea is to truncate the von Neumann entropy as a linear combination of higher-order state overlaps, i.e., $\mathrm{tr}(\rho^k)$, and estimate each $\mathrm{tr}(\rho^k)$ via quantum gadgets, e.g., the swap test, respectively. Next, we employ a classical optimizer to minimize the loss function via tuning the parameters and then use the optimized circuit to prepare the target Gibbs state. Note that the subroutine of loss evaluation occurs on the quantum devices, and the procedure of optimization is entirely classical. Then, classical optimization tools such as gradient-based or gradient-free methods can be employed in the optimization loop.

In general, the variational quantum circuit contains a series of parameterized single-qubit Pauli rotation operators and controlled-NOT (CNOT) or CZ gates alternately [47]. Here we follow this circuit pattern and mainly use Pauli-Y rotation operators and CNOT gates. For the optimization part, a variety of approaches have been proposed to optimize such variational quantum circuits, including Nelder-Mead [48,49], Monte Carlo [50], quasi-Newton [48], gradient descent [51], and Bayesian methods. Here we choose ADAM [52] as our gradient-based optimizer in the numerical experiments.

1: Input: choose the ansatz of unitary $U(\boldsymbol{\theta})$, tolerance ε, truncation order 2, and initial parameters of $\boldsymbol{\theta}$;
2: Compute coefficients C_0, C_1, C_2 according to Eq. (7).
3: Prepare the initial states $|00\rangle$ in registers AB and apply $U(\boldsymbol{\theta})$.
4: Measure and compute $\mathrm{tr}(H\rho_{B_1})$ and compute the loss function $L_1 = \mathrm{tr}(H\rho_{B_1})$;
5: Measure and compute $\mathrm{tr}(\rho_{B_2}\rho_{B_3})$ via Destructive Swap Test and compute the loss function $L_2 = -\beta^{-1}C_1\,\mathrm{tr}(\rho_{B_2}\rho_{B_3})$;
6: Measure and compute $\mathrm{tr}(\rho_{B_4}...\rho_{B_6})$ via higher-order state overlap estimation and compute the loss function $L_3 = -\beta^{-1}C_2\,\mathrm{tr}(\rho_{B_4}...\rho_{B_6})$.
7: Perform optimization of $\mathcal{F}_2(\boldsymbol{\theta}) = \sum_{k=1}^{3} L_k - \beta^{-1}C_0$ and update parameters of $\boldsymbol{\theta}$;
8: Repeat 3-7 until the loss function $\mathcal{F}_2(\boldsymbol{\theta})$ converges with tolerance ε;
9: Output: the state $\rho^{out} = \mathrm{tr}_A\, U(\boldsymbol{\theta})\,|00\rangle\langle 00|_{AB}\, U(\boldsymbol{\theta})^\dagger$.

Algorithm 1. Variational quantum Gibbs state preparation with truncation order 2

For simplicity, the overall hybrid algorithm with the two-order loss function is given in Algorithm 1, and a picture for illustration is depicted in Fig. 1. The variational quantum algorithm for general truncation order K is deferred to Appendix A.

Clearly, Algorithm 1 can be efficiently implemented on near-term quantum devices since the estimation of

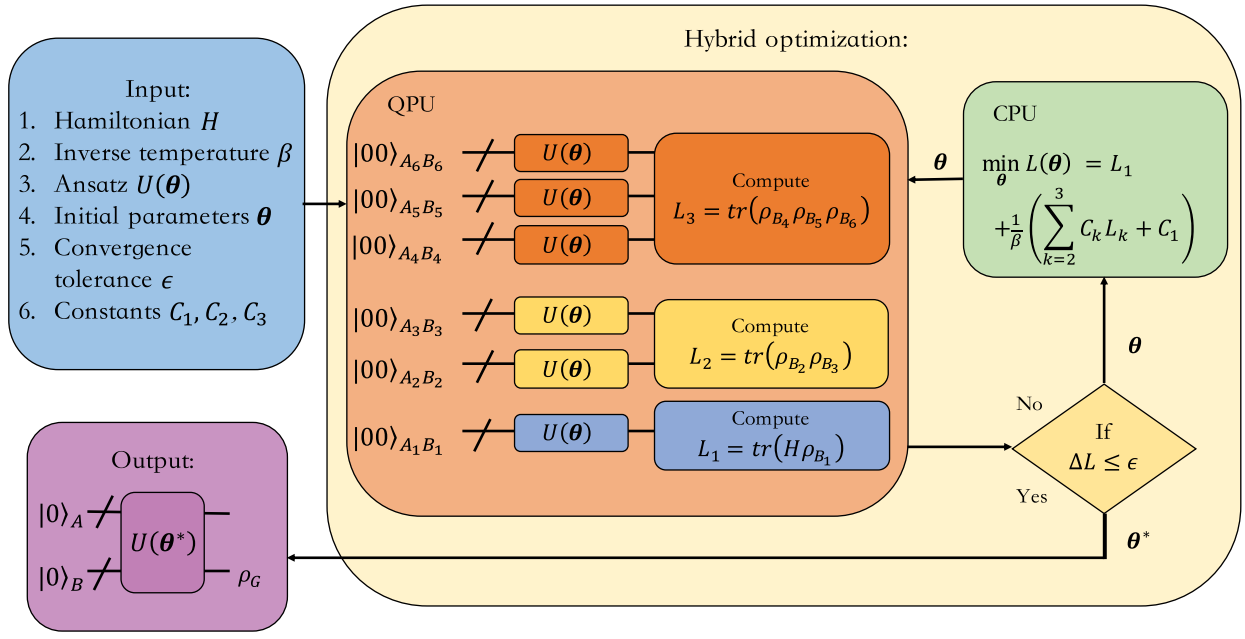

FIG. 1. Schematic representation of the variational quantum Gibbs state preparation with truncation order 2. First, we prepare the Hamiltonian H and inverse temperature β and then send them into the hybrid optimization. Second, we choose an ansatz and employ it to evaluate the loss functions L_1, L_2, L_3 on quantum devices. Then we calculate the difference $\Delta\mathcal{F}_2(\boldsymbol{\theta})$ using L_1, L_2, L_3. Next, if the condition $\Delta\mathcal{F}_2 \le \epsilon$ is not satisfied then we perform classical optimization to update parameters $\boldsymbol{\theta}$ of the ansatz and return to the loss evaluation. Otherwise, we output the current parameters $\boldsymbol{\theta}^*$, which could be used to prepare Gibbs state ρ_G via $U(\boldsymbol{\theta})$. Here in the quantum device, registers A_2, B_2, A_3, B_3 are used to evaluate $\mathrm{tr}\,(\rho_{B_2}\rho_{B_3})$ and registers $A_4, B_4, \ldots, A_6, B_6$ are used to evaluate $\mathrm{tr}\,(\rho_{B_4}\rho_{B_5}\rho_{B_6})$.

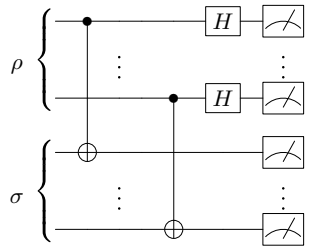

FIG. 2. Quantum circuit for implementing the destructive swap test. In the circuit, two states ρ and σ are prepared at different registers. Then CNOT and Hadamard gates are performed as shown. The state overlap can be estimated via postprocessing.

loss function $\mathcal{F}_2$ only requires measuring the expected value $\langle H\rangle_\rho$, the purity or the state overlap $\mathrm{tr}(\rho^2)$, and the higher-order state overlap $\mathrm{tr}(\rho^3)$. To compute the state overlap, one approach is to utilize the well-known swap test [53,54], which has a simple physical implementation in quantum optics [55,56] and can be experimentally implemented on near-term quantum hardware [34,57,58]. For instance, we could use a variant version of the swap test (see Fig. 2), called the destructive swap test [56,59]. Compared to the general swap test, the destructive swap test is more practical on near-term devices, since it is ancilla-free and costs less circuit depth and fewer gates. Using the circuit in Fig. 2, the quantity $\mathrm{tr}(\rho^2)$ is expected to be estimated on near-term quantum hardware.

Regarding higher-order state overlaps, e.g., $\mathrm{tr}(\rho^3)$, there are methods that use a similar circuit to that used for the destructive swap test [60], whose depth is only 2. For more information, see Ref. [60]. We can also use the qubit-efficient circuit proposed by Yirka *et al.* [61] to compute $\mathrm{tr}(\rho^k)$ for larger k. In particular, the circuit only uses a

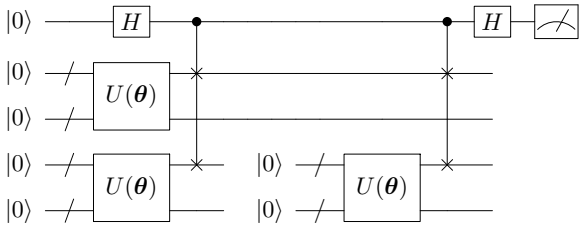

FIG. 3. Quantum circuit for computing $\mathrm{tr}(\rho^3)$. In the circuit, $U(\boldsymbol{\theta})$ denotes the state preparation circuit and H denotes the Hadamard gate. Four registers are used to prepare states by $U(\boldsymbol{\theta})$, and one ancillary qubit is used to perform the controlled swap operator. The qubit reset occurs on the bottom two registers, where the break in the wire represents the reset operation. Notably, the state on the bottom two registers is first implemented with a circuit $U(\boldsymbol{\theta})$ and controlled swap operator and then reset to state $|0\rangle$. Again, $U(\boldsymbol{\theta})$ and the controlled swap operator are performed on the bottom registers. Finally, $\mathrm{tr}(\rho^3)$ can be obtained via postprocessing the measurement results.

constant number of qubits, where the key is that some subset of qubits can be reset in the course of quantum computation. For convenience, we call this method the higher-order state overlap estimation and provide an example for computing $\mathrm{tr}(\rho^3)$ in Fig. 3. We also refer interested readers to Ref. [61] for more details on qubit-efficient algorithms for computing $\mathrm{tr}(\rho^k)$. Hence, using these qubit-efficient quantum circuits will significantly circumvent our approach's resource requirements for computing $\mathrm{tr}(\rho^k)$ for $k \geq 3$ and enable our approach to be implementable on noisy intermediate-scale quantum (NISQ) computers.

B. Performance analysis of our method

In this section, we analyze the performance of our variational algorithm. Specifically, we first define a formal optimization problem that aims to find the global minimum of the truncated free energy. Second, we show that the prepared state has a higher overlap with the desired Gibbs state, using higher-order loss functions in our approach.

1. Loss function

In our algorithm (Algorithm 2 in Appendix A), the K-truncated free energy $\mathcal{F}_K$ is taken as the loss function. To find the global minimum of the loss function $\mathcal{F}_K$, we update the parameters $\boldsymbol{\theta}$ till the termination condition is reached. We denote the obtained optimal parameters by $\boldsymbol{\theta}_{\mathrm{opt}}$. Then we can prepare an approximation operator for the Gibbs state by performing the parameterized circuit $U(\boldsymbol{\theta}_{\mathrm{opt}})$.

The loss function $\mathcal{F}_K$ is obtained by truncating the Taylor series of von Neumann entropy at order K. Specifically, let $K \in \mathbb{Z}_+$ be a positive integer, and denote the truncated entropy by $S_K(\rho)$. Let H denote the Hamiltonian, and let $\beta > 0$ be the inverse temperature. Then the loss function $\mathcal{F}_K(\boldsymbol{\theta})$ is defined as

$$\mathcal{F}_K(\boldsymbol{\theta}) = \mathrm{tr}[H\rho(\boldsymbol{\theta})] - \beta^{-1} S_K[\rho(\boldsymbol{\theta})]. \tag{5}$$

Here the free energy is determined by parameters $\boldsymbol{\theta}$, since the state $\rho(\boldsymbol{\theta})$ is prepared by the PQC $U(\boldsymbol{\theta})$. The K-truncated entropy $S_K(\rho)$ is given as

$$S_K(\rho) = \sum_{k=1}^{K} \frac{(-1)^k}{k} \mathrm{tr}[(\rho - I)^k \rho] = \sum_{j=0}^{K} C_j \,\mathrm{tr}(\rho^{j+1}). \tag{6}$$

In Eq. (6), the C_j coefficients of $S_K(\rho)$ are given in the form

$$C_0 = \sum_{k=1}^{K} \frac{1}{k}, \quad C_j = \sum_{k=j}^{K} \binom{k}{j} \frac{(-1)^j}{k}, \quad C_K = \frac{(-1)^K}{K}, \tag{7}$$

where $j = 1, \ldots, K-1$.

Recall that our goal is to find parameters $\boldsymbol{\theta}_{\text{opt}}$ that minimize the value of the loss function $\mathcal{F}_K(\boldsymbol{\theta})$, i.e., $\boldsymbol{\theta}_{\text{opt}} = \text{argmin}_{\boldsymbol{\theta}} \mathcal{F}_K(\boldsymbol{\theta})$. In practice, the optimization loop only terminates if some condition given previously is reached. Therefore, one cannot obtain the true optimum, but some parameters $\boldsymbol{\theta}_0$ that will approximately minimize the loss function in the sense that

$$\mathcal{F}_K(\boldsymbol{\theta}_0) \leq \min_{\boldsymbol{\theta}} \mathcal{F}_K(\boldsymbol{\theta}) + \epsilon, \tag{8}$$

where ϵ is the error tolerance in the optimization problem. Specifically, we assume that the used PQC $U(\boldsymbol{\theta})$ endows sufficient expressiveness to prepare the desired Gibbs state or a state very close to it. Hence, the state $\rho(\boldsymbol{\theta}_0)$ could be taken to approximate the desired Gibbs state.

2. Error analysis

Since the loss function $\mathcal{F}_K(\boldsymbol{\theta})$ is a truncated version of the free energy, the solution $\boldsymbol{\theta}_0$ to the optimization problem in Eq. (8) is not exactly the quantum Gibbs state ρ_G. However, the obtained state $\rho(\boldsymbol{\theta}_0)$ is not far away from the Gibbs state ρ_G. Here, we use the fidelity to characterize the distance between two states. In the following, we show the validity of this claim by providing a lower bound on the fidelity between $\rho(\boldsymbol{\theta}_0)$ and ρ_G in Theorem 1 below. In particular, the result in Theorem 1 implies that the larger the truncation order K, the closer the state $\rho(\boldsymbol{\theta}_0)$ is to the state ρ_G.

Theorem 1: *Given a positive integer K and error tolerance $\epsilon > 0$, let $\beta > 0$ be the inverse temperature and $\boldsymbol{\theta}_0$ be the solution to the optimization in Eq. (8). Assume that the rank of the output state $\rho(\boldsymbol{\theta}_0)$ is r; then the fidelity between the state $\rho(\boldsymbol{\theta}_0)$ and the Gibbs state ρ_G is lower bounded as*

$$F[\rho(\boldsymbol{\theta}_0), \rho_G] \geq 1 - \sqrt{2\left(\beta\epsilon + \frac{2r}{K+1}(1-\Delta)^{K+1}\right)}, \tag{9}$$

where $\Delta \in (0, e^{-1})$ is a constant determined by K.

Theorem 1 implies that we can regard the output state $\rho(\boldsymbol{\theta}_0)$ as an approximation for the Gibbs state for a given error tolerance in the optimization problem and a truncation order K. The quantity on the right-hand side of Eq. (9) quantifies the extent that $\rho(\boldsymbol{\theta}_0)$ approximates ρ_G. Also, we can easily see that the quantity becomes larger when the order K increases.

Next, we prove Theorem 1 by building a connection between the relative entropy and the fidelity and then deriving an upper bound on the truncation error.

Lemma 1: *Given quantum states ρ and σ and a constant $\delta > 0$, suppose that the relative entropy $S(\rho\|\sigma)$ is less than δ, i.e., $S(\rho\|\sigma) \leq \delta$. Then the fidelity between ρ and σ is lower bounded. To be specific, $F(\rho, \sigma) \geq 1 - \sqrt{2\delta}$.*

Proof: Recall the relationship between the trace distance and the fidelity $D(\rho, \sigma) \geq 1 - F(\rho, \sigma)$, and Pinsker's inequality $D(\rho, \sigma) \leq \sqrt{2S(\rho\|\sigma)}$; then we have the inequality

$$F(\rho, \sigma) \geq 1 - D(\rho, \sigma) \geq 1 - \sqrt{2S(\rho\|\sigma)} \geq 1 - \sqrt{2\delta}, \tag{10}$$

completing the proof. ■

Lemma 1 states that, if one wants to lower bound the fidelity $F[\rho(\boldsymbol{\theta}_0), \rho_G]$ between the obtained state $\rho(\boldsymbol{\theta}_0)$ and the Gibbs state ρ_G, then it suffices to upper bound the relative entropy $S[\rho(\boldsymbol{\theta}_0)\|\rho_G]$ between them. Thus we proceed to give an upper bound of the relative entropy.

Let δ_0 be the truncation error of $S_K(\rho)$. Then the definition of the free energy allows us to bound the difference between the free energy and its truncated version, i.e., $|\mathcal{F}_K(\rho) - \mathcal{F}(\rho)| \leq \beta^{-1}\delta_0$. Recall the well-known free-energy equation, $\mathcal{F}(\rho) = \mathcal{F}(\rho_G) + \beta^{-1}S(\rho\|\rho_G)$, which indicates that, for arbitrary density ρ, the free energy $\mathcal{F}(\rho)$ can be represented as a linear combination of the free energy $\mathcal{F}(\rho_G)$ of the quantum Gibbs state ρ_G and the relative entropy between ρ and ρ_G. Therefore, an upper bound on the relative entropy $S[\rho(\boldsymbol{\theta}_0)\|\rho_G]$ is readily derived as

$$\begin{aligned} S[\rho(\boldsymbol{\theta}_0)\|\rho_G] &= \beta|\mathcal{F}[\rho(\boldsymbol{\theta}_0)] - \mathcal{F}(\rho_G)| \\ &= \beta|\mathcal{F}[\rho(\boldsymbol{\theta}_0)] - \mathcal{F}_K[\rho(\boldsymbol{\theta}_0)] \\ &\quad + \mathcal{F}_K[\rho(\boldsymbol{\theta}_0)] - \mathcal{F}(\rho_G)| \\ &= \delta_0 + \beta|\mathcal{F}_K[\rho(\boldsymbol{\theta}_0)] - \mathcal{F}(\rho_G)| \\ &\leq 2\delta_0 + \beta\epsilon, \end{aligned} \tag{11}$$

where the inequality in Eq. (11) is due to the fact that $\mathcal{F}(\rho_G) \leq \mathcal{F}_K[\rho(\boldsymbol{\theta}_0)] \leq \mathcal{F}(\rho_G) + \beta^{-1}\delta_0 + \epsilon$, which is stated in Lemma 2 below and proved in Appendix B 1. In particular, to obtain the result in Lemma 2, we assume that the used PQC is expressive enough to prepare the target Gibbs state or a state very close to it.

Lemma 2: *Given the error tolerance $\epsilon > 0$ in the optimization problem in Eq. (8), suppose that the truncation error of the free energy is $\beta^{-1}\delta_0 > 0$. Then we can derive the following relation between $\mathcal{F}(\rho_G)$ and $\mathcal{F}_K[\rho(\boldsymbol{\theta}_0)]$, where $\boldsymbol{\theta}_0$ is the output of the optimization and ρ_G is the Gibbs state:*

$$\mathcal{F}(\rho_G) \leq \mathcal{F}_K(\boldsymbol{\theta}_0) \leq \mathcal{F}(\rho_G) + \beta^{-1}\delta_0 + \epsilon. \tag{12}$$

Now, given the truncation order K, we derive an upper bound on the difference between $S_K(\rho)$ and $S(\rho)$ in the following lemma and defer the proof to Appendix B 2.

Lemma 3: *Given a quantum state ρ, assume that the truncation order of the truncated von Neumann entropy is $K \in \mathbb{Z}_+$, and choose $\Delta \in (0, e^{-1})$ such that $-\Delta \ln(\Delta) < 1/K + 1(1-\Delta)^{K+1}$. Let δ_0 denote the truncation error, i.e., the difference between the von Neumann entropy $S(\rho)$ and its K-truncated entropy $S_K(\rho)$. Then the truncated error δ_0 is upper bounded in the sense that*

$$\delta_0 \leq \frac{r}{K+1}(1-\Delta)^{K+1}, \tag{13}$$

where r denotes the rank of the density operator.

Replacing δ_0 in Eq. (11) with its upper bound in Eq. (13) immediately leads to a bound on the relative entropy $S[\rho(\boldsymbol{\theta}_0)\|\rho_G]$. Taking this bound into Lemma 1, a lower bound on the fidelity $F[\rho(\boldsymbol{\theta}), \rho_G]$ is then derived, which is exactly that in Eq. (9). This completes the proof of Theorem 1.

C. Optimization via the gradient-based method

Finding optimal parameters $\boldsymbol{\theta}_{\text{opt}}$ is a major part of our variational algorithm. Both gradient-based and gradient-free methods could be used to do the optimization. Here, we provide analytical details on the gradient-based approach, and we refer the reader to Ref. [47] for more information on the optimization subroutines in variational quantum algorithms.

The choice of truncation order K could be various and depends on the required accuracy for Gibbs state preparation. Here we mainly focus on the two-order loss function $\mathcal{F}_2(\boldsymbol{\theta})$ as higher fidelity could be expected by the result in Theorem 1. We numerically show the validity of this choice in the next section. In particular, the numerical results show that we can use a two-order loss function to prepare high-fidelity Gibbs states of several many-body Hamiltonians.

Now, we show that $\mathcal{F}_2(\boldsymbol{\theta})$ is convex, which indicates that the gradient-based method could efficiently minimize it. We also derive the analytical expressions for its gradients and show that these analytical gradients could also be evaluated efficiently on NISQ devices. Notably, the same circuit for estimating $\mathcal{F}_2(\rho)$ can also be used to calculate their gradients.

1. Convexity of 2-truncated free energy

Recall the definition of the K-truncated entropy $S_K(\rho)$ in Eq. (6); in this section, we take $K = 2$. Given truncation order 2, the loss function $\mathcal{F}_2(\rho)$ is of the form

$$\mathcal{F}_2(\boldsymbol{\theta}) = \text{tr}[H\rho(\boldsymbol{\theta})] + \beta^{-1}\left(2\,\text{tr}[\rho(\boldsymbol{\theta})^2] - \frac{1}{2}\,\text{tr}[\rho(\boldsymbol{\theta})^3] - \frac{3}{2}\right). \tag{14}$$

Note that the functional $\text{tr}(H\rho)$ is linear for a given Hamiltonian H and $\beta > 0$; therefore, the convexity of loss function $\mathcal{F}_2$ is determined by the convexity of the functional $g(\rho) = 2\,\text{tr}(\rho^2) - \frac{1}{2}\,\text{tr}(\rho^3) - \frac{3}{2}$. Hence, to prove the convexity of $\mathcal{F}_2$, we only need to show the convexity of functional $g(\rho)$.

Lemma 4: *The functional $g(\rho) = 2\,\text{tr}(\rho^2) - \frac{1}{2}\,\text{tr}(\rho^3) - \frac{3}{2}$ is convex, where ρ is a density operator.*

Proof: According to Theorem 2.10 of Ref. [62], the functional $\text{tr}[f(\rho)]$ is convex if the associated function $f : \mathbb{R} \to \mathbb{R}$ is convex. In the scenario where $\mathcal{F}_2(\rho)$ is given in Eq. (14), the associated function of g is defined as $f(x) = 2x^2 - \frac{1}{2}x^3 - \frac{3}{2}$ for all $x \in [0, 1]$. The claim follows upon proving that f is convex, and the second-order derivative $f^{(2)}$ of f is positive, since

$$f^{(2)}(x) = 4 - 3x \geq 1 \quad \text{for all } x \in [0, 1]. \tag{15}$$

Therefore, the positivity of the second-order derivative of f leads to the convexity of $\mathcal{F}_2(\rho)$ in the set of density operators. ■

2. Analytical gradient

Here we discuss the computation of the gradient of the global loss function $\mathcal{F}_2(\boldsymbol{\theta})$. Inspired by previous works [63–65], we compute the gradients of the 2-truncated free energy $\mathcal{F}_2$ by shifting the parameters of the same circuit for estimating $\mathcal{F}_2$. Note that there is an alternative method to estimate the partial derivative with a single circuit [66], but at the cost of using an ancillary qubit.

In Fig. 1, the density operator $\rho(\boldsymbol{\theta})$ is prepared in the register B by performing a sequence of unitaries $U = U_N \cdots U_1$ on the state $|00\rangle_{AB}$ in registers AB. Each gate U_m is either fixed, e.g., a CNOT gate, or parameterized. The parameterized gates are of the form $U_m = e^{-iH_m\theta_m/2}$, where the θ_m are real parameters and H_m is a tensor product of Pauli matrices. Then the loss function $\mathcal{F}_2$ is related to parameters $\boldsymbol{\theta}$, and its gradient is explicitly given by

$$\nabla_{\boldsymbol{\theta}}\mathcal{F}_2(\boldsymbol{\theta}) = \left(\frac{\partial\mathcal{F}_2(\boldsymbol{\theta})}{\partial\theta_1}, \ldots, \frac{\partial\mathcal{F}_2(\boldsymbol{\theta})}{\partial\theta_N}\right). \tag{16}$$

The partial derivatives of $\mathcal{F}_2$ with respect to θ_m is

$$\begin{aligned}\frac{\partial\mathcal{F}_2(\boldsymbol{\theta})}{\partial\theta_m} = {} & \frac{1}{2}(\langle K\rangle_{\theta_m+\pi/2} - \langle K\rangle_{\theta_m-\pi/2}) \\ & + \beta^{-1}\Big[2(\langle O\rangle_{\theta_m+\pi/2,\theta_m} - \langle O\rangle_{\theta_m-\pi/2,\theta_m}) \\ & - \frac{3}{4}(\langle G\rangle_{\theta_m+\pi/2,\theta_m,\theta_m} - \langle G\rangle_{\theta_m-\pi/2,\theta_m,\theta_m})\Big],\end{aligned} \tag{17}$$

where $\langle K\rangle$, $\langle O\rangle$, and $\langle G\rangle$ are used to estimate $\text{tr}[H\rho(\boldsymbol{\theta})]$, $\text{tr}[\rho(\boldsymbol{\theta})^2]$, and $\text{tr}[\rho(\boldsymbol{\theta})^3]$, respectively, and their definitions

are given as

$$\langle K\rangle_{\theta_\alpha} = \mathrm{tr}(U_\alpha \psi_{A_1B_1} U_\alpha^\dagger \times K), \tag{18}$$

$$\langle O\rangle_{\theta_\alpha,\theta_\beta} = \mathrm{tr}\left(\left[\bigotimes_{l=2}^{3} U_\alpha \psi_{A_lB_l} U_\alpha^\dagger\right] \times O\right), \tag{19}$$

$$\langle G\rangle_{\theta_\alpha,\theta_\beta,\theta_\gamma} = \mathrm{tr}\left(\left[\bigotimes_{l=4}^{6} U_\alpha \psi_{A_lB_l} U_\alpha^\dagger\right] \times G\right). \tag{20}$$

Here, we defer the definitions of the K, O, G notation and the process of deriving the gradient to Appendix B 4. From Eq. (17), we can see that the gradient can be efficiently computed by shifting the parameters in the loss function.

To summarize, the above results entail that the partial derivatives of our loss function $\mathcal{F}_2(\boldsymbol{\theta})$ with respect to $\boldsymbol{\theta}$ are completely determined by Eq. (17). This indicates that the analytical gradient of our loss function $\mathcal{F}_2(\boldsymbol{\theta})$ can be efficiently computed on near-term quantum devices by shifting parameters and performing measurements. With the analytical gradients, one could apply the gradient-based methods to minimize the loss function. Specifically, parameters $\boldsymbol{\theta}$ in the unitary $U(\boldsymbol{\theta})$ are updated towards the steepest direction of the loss function, i.e., $\boldsymbol{\theta} \leftarrow \boldsymbol{\theta} - \eta\nabla_{\boldsymbol{\theta}}\mathcal{F}_2(\boldsymbol{\theta})$, where $\nabla_{\boldsymbol{\theta}}\mathcal{F}_2(\boldsymbol{\theta})$ is the gradient vector and η is the learning rate that determines the step sizes. Under suitable assumptions, the loss functions converge to the global minimum after certain iterations of the above procedure. Note that other gradient-based methods, e.g., stochastic gradient descent, ADAM [52], can also be used in the optimization loop of our variational Gibbs state preparation algorithm.

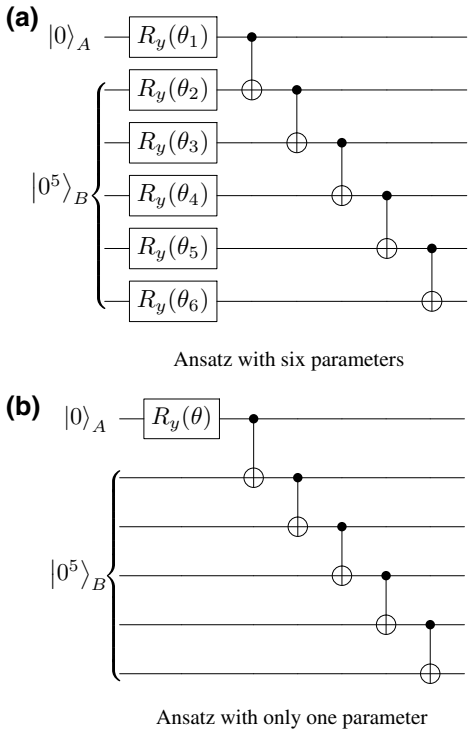

FIG. 4. Two ansatzes for the Ising chain model. These ansatzes are composed of two registers A and B, where one ancillary qubit is set in A and five qubits are set in B. Notably, the qubits in B are performed with rotations $R_y(\theta)$ and CNOT gates in (a), and only CNOT gates in (b).

III. NUMERICAL SIMULATIONS

In this section we discuss conducting numerical experiments to prepare the Gibbs states of two common Hamiltonian examples: the Ising chain model and XY spin-$\frac{1}{2}$ chain model. In Sec. III A, we study the Ising chain model and show that a parameterized circuit with one ancillary qubit and shallow depth could be trained to produce the Ising Gibbs state with fidelity higher than 99%, especially at

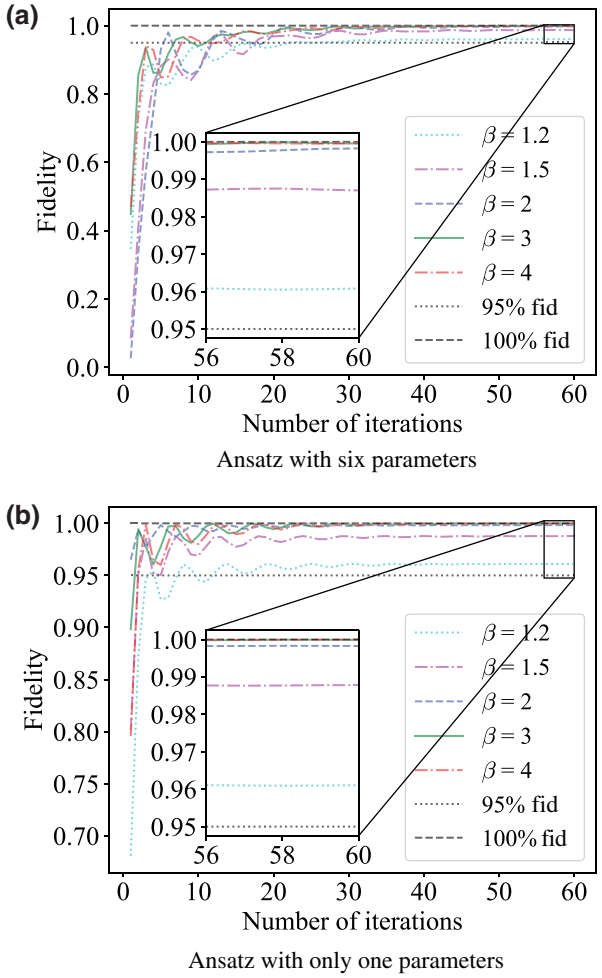

FIG. 5. Fidelity curves for the Ising chain Gibbs state preparation with different β. In (a), we use the ansatz with six parameters [cf. Fig. 4(a)]; in (b), we use the ansatz with only one parameter [cf. Fig. 4(b)]. We can see that they have almost the same performance, which indicates that one parameter is enough for this task.

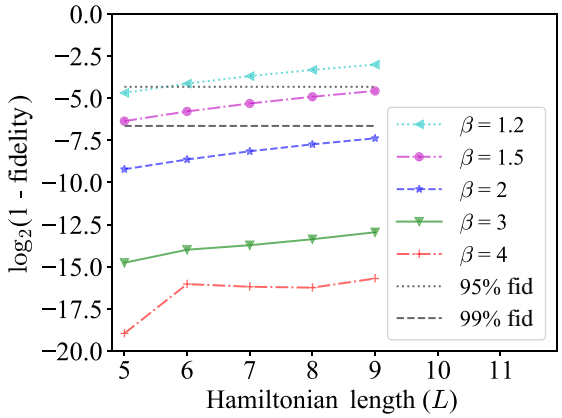

FIG. 6. Semilog plot of the fidelity versus the Ising Hamiltonian length (L) with different β for the Ising chain model. Here, $\log_2$ is the logarithm to the base 2. We can see that the fidelity increases exponentially with increasing β.

higher β or lower inverse temperature ($\beta \geq 2$). Furthermore, we also give a more sophisticated ansatz with only one parameter that can do the same thing. As a second example, in Sec. III B, we study the spin chain model. We show that our approach could achieve a fidelity higher than 95% via an ansatz with 30 parameters for $\beta \geq 1.5$ for a five-length XY spin-$\frac{1}{2}$ chain Hamiltonian. In particular, the fidelity could also achieve 99% for the lower inverse temperature case. In our numerical experiments, the classical parameters of the parameterized circuits are initialized from a uniform distribution in $[0, 2\pi]$, and then updated via the ADAM gradient-based method [52] until the loss function converges.

A. Ising model

As our first example, we consider the spin-$\frac{1}{2}$ chain B of length $L = 5$, with the Ising Hamiltonian

$$H_B = -\sum_{i=1}^{L} Z_{B,i} Z_{B,i+1} \tag{21}$$

and periodic boundary conditions (i.e., $Z_{B,6} = Z_{B,1}$). Our goal is to prepare the corresponding Gibbs state

$$\rho_G = e^{-\beta H_B} / \operatorname{tr}(e^{-\beta H_B}). \tag{22}$$

To prepare this state, we choose a six-qubit parameterized circuit with $n_A = 1$ and $n_B = 5$ (cf. Fig. 4), where A is the ancillary system used to produce a mixed state on system B. Here we need to note that we only use a one-qubit ancillary system in our ansatz, which is significantly less than in Ref. [36] where $n_A = n_B$. In Fig. 4(a), the ansatz consists of six single-qubit Pauli-Y rotation operators with different classic parameters θ_i ($i \in [6]$) and five CNOT gates.

After applying this ansatz on the input zero state $|0\rangle_A |0^5\rangle_B$, we can get the output state on system B, which is desired to get close to the Gibbs state in Eq. (22). The fidelity between this output state and the Gibbs state, in the training process with different β, is depicted in Fig. 5(a). When $\beta \geq 1.2$, after 30 iterations of updating parameters, our method can easily achieve a fidelity higher than 95%. Specifically, if $\beta \geq 2$, the fidelity is higher than 99%, which indicates that our approach can almost exactly prepare the Gibbs state in Eq. (22), especially at higher inverse temperatures.

We also test the preparation of the Ising Gibbs state for different lengths (i.e., $L = 5, 6, 7, 8, 9$), and all of the ansatzes are similar to Fig. 4(a), which only uses one additional qubit. The curves of the logarithmic form of the fidelity between the output state ρ_B and the Gibbs state ρ_G are depicted in Fig. 6. We can intuitively see that the larger the Hamiltonian length, the lower fidelity we achieve. However, we also find that the temperature has a significant impact on fidelity: the larger β, the higher the fidelity (see Proposition 2 below for a detailed analysis). In particular, when $\beta \geq 2$, the fidelity is already higher than 99% for the Hamiltonian length listed in the figure.

An interesting experimental phenomenon in the training process is that the first parameter θ_1 in system A approaches $\pi/2$ while other parameters in system B approach 0. Hence, we update the ansatz to a simplified one in Fig. 4(b)

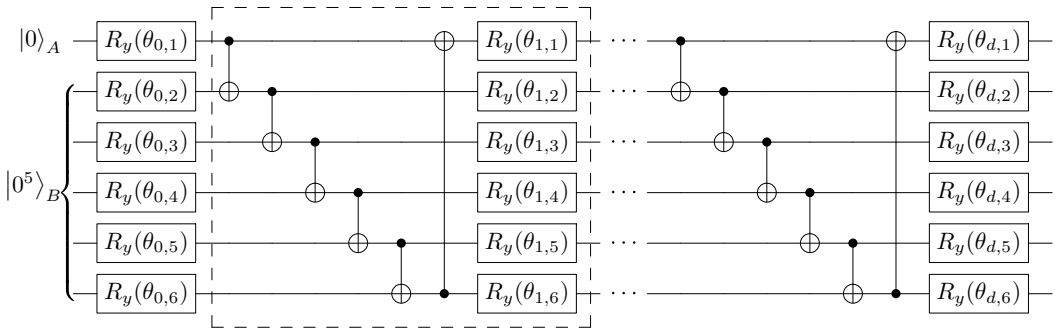

FIG. 7. The ansatz for the XY spin-$\frac{1}{2}$ chain model. This ansatz contains one ancilla qubit in register A and five qubits in register B. Rotation gates $R_y(\theta)$ are first applied on all qubits. Then, a basic circuit module (highlighted in the dashed box) composed of CNOT gates and rotation gates $R_y(\theta)$ is repeatedly applied. Here, d means repeating d times.

and implement the numerical simulations in Fig. 5(b). Notably, the overall performance is almost the same as using the ansatz with six parameters [cf. Fig. 5(a)]. To further explore this interesting behavior of the Ising chain Gibbs state preparation, we analyze the states generated using different loss functions.

Proposition 1: *Consider the circuit in Fig. 4(b) and let* $\rho_B(\theta)$ *be its output state on system B. For the Ising chain model, if we compute its free energy in Eq. (3) and our truncated cost in Eq. (5), then the optimal parameters that minimize these two loss functions are both* $\theta = \pi/2 + k\pi$, *where* $k \in \mathbb{Z}$. *As a result,* $\rho_B(\pi/2)$ *is the best state, under this circuit, that approaches the Gibbs state in Eq. (22), with a fidelity larger than 95% for any* $\beta \geq 1.25$.

We defer the proof of Proposition 1 to Appendix B 5. Here, we need to note that this fidelity is just a lower bound; actually, when $\beta = 1.2$, we have still achieved a fidelity greater than 95% for $n_B = 5$, as demonstrated in our experiments. Furthermore, in Proposition 1 the number of qubits in system B is not limited to five, instead it can be any positive integer greater than 2.

Another interesting experimental result (cf. Fig. 6) shows that the fidelity between the Ising chain Gibbs state ρ_G and the output state ρ_B of our method increases exponentially when β increases. The result is as follows, and the details can be found in Appendix B 6.

Proposition 2: *Consider the circuit in Fig. 4(b) and let* $\rho_B(\theta)$ *be its output state on system B. Then the fidelity between* $\rho_B(\pi/2)$ *and the Gibbs state* ρ_G *is lower bounded. To be more specific,*

$$F\left[\rho_B\left(\frac{\pi}{2}\right), \rho_G\right] \geq \frac{1}{\sqrt{1 + (N/2 - 1)e^{-\beta\Delta}}}, \tag{23}$$

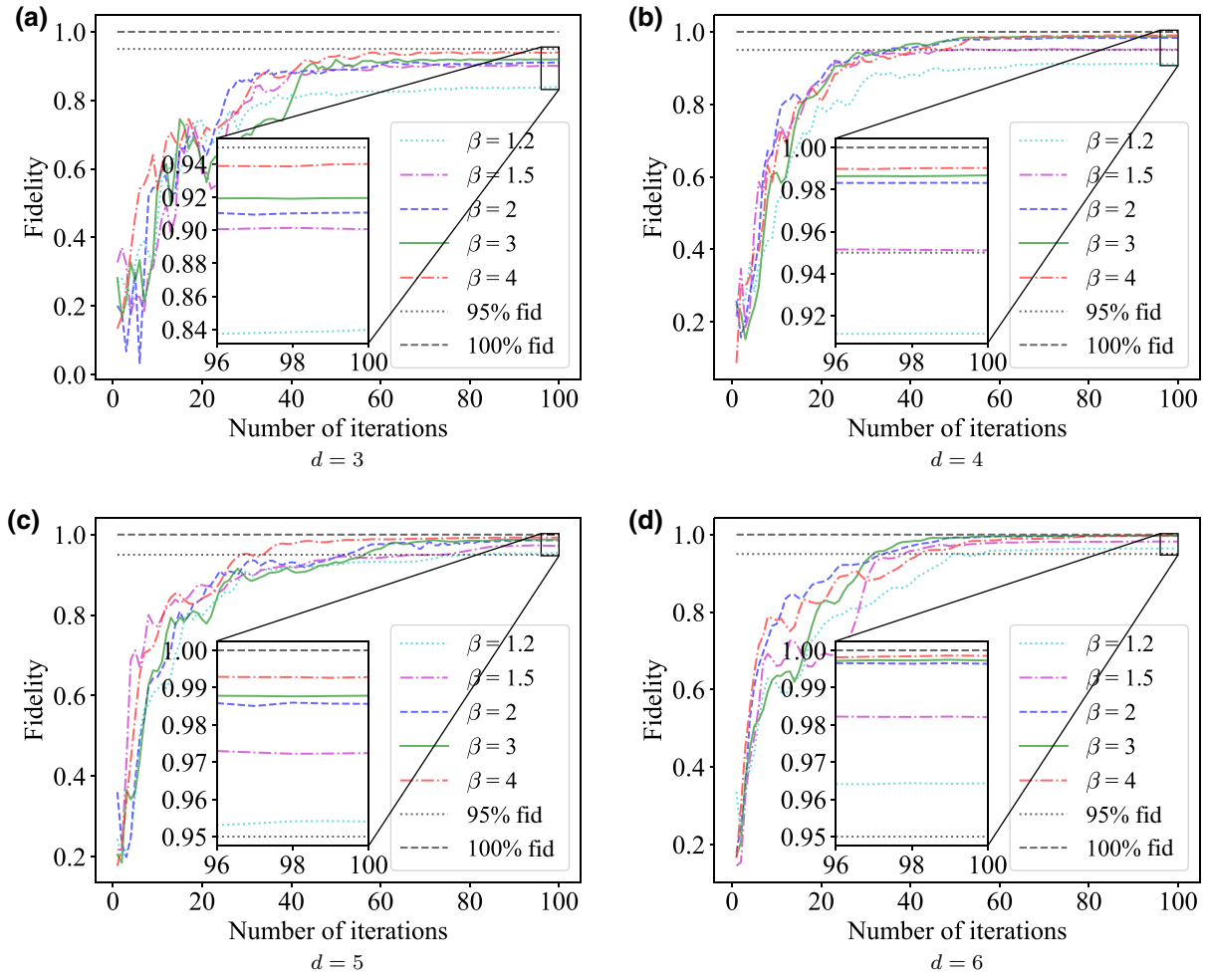

FIG. 8. Fidelity curves for the XY spin-$\frac{1}{2}$ chain Gibbs state preparation with different β. The results of the fidelity obtained with different β are represented by colored lines. In (a)–(d), numerical experiments are performed using different ansatzes. In each ansatz, the basic circuit module (cf. Fig. 7) is repeated different times, i.e., d. Note that each ansatz has $(n_A + n_B)(d + 1) = 6(d + 1)$ parameters. Here better performance is obtained with larger d.

where N is the dimension of system B, i.e., $N = 2^{n_B}$, and Δ is the spectral gap of H_B on system B, i.e., the discrepancy between the minimum and the second minimum eigenvalues.

Notably, our approach can prepare the Gibbs state with high accuracy for large β. This is because the fidelity $F[\rho_B(\pi/2), \rho_G]$ converges fast to 1 with increasing β.

B. *XY* spin-$\frac{1}{2}$ chain model

Our second instance is the *XY* spin-$\frac{1}{2}$ chain B of length $L = 5$, with the Hamiltonian $H_B = -\sum_{i=1}^{L} X_{B,i}X_{B,i+1} + Y_{B,i}Y_{B,i+1}$ and periodic boundary conditions (i.e., $Z_{B,6} = Z_{B,1}$). To prepare the spin chain Gibbs state, we first choose a six-qubit parameterized circuit with $n_A = 1$ and $n_B = 5$ (cf. Fig. 7), where the basic circuit module (which contains a CNOT layer and a layer of single-qubit Pauli-Y rotation operators) is repeated d times, and the total number of parameters of this circuit is $(n_A + n_B)(d + 1)$.

The fidelity between the output state of this circuit and the Gibbs state is shown in Fig. 8, where different d values are included. We see that, when $d \geq 4$ and $\beta \geq 1.5$, our approach can easily achieve a fidelity greater than 95%, and if $\beta \geq 2$, the fidelity could be higher than 98%. Furthermore, if β is equal to 4, the fidelity can be even higher than 99%, which means that our approach could almost generate the Gibbs state exactly in higher β (or lower temperature). One possible reason that we need larger d for this instance is that these Hamiltonians are not directly generated via the CNOT module. Hence we need multiple CNOT modules to fully entangle the state.

We note that the above experiments mainly focus on lower temperatures, i.e., $\beta > 1$, where smaller ancillary systems and the lower truncation order $K = 2$ are usually sufficient to achieve a higher fidelity. In order to test our algorithm's performance with different truncation orders K under higher temperatures (e.g., $\beta < 0.5$), we choose a six-qubit parameterized circuit with $n_A = 3$ and $n_B = 3$ for a three-length *XY* spin-$\frac{1}{2}$ chain Hamiltonian. Here, the ansatz is similar to Fig. 7 and we set $d = 8$ to make it expressive enough. By $n_A = n_B$ we mean that the ancillary systems can cover all the Hamiltonian's ranks. The boxplots of the fidelity versus various truncation orders K are illustrated in Fig. 9, where three higher temperatures ($\beta = 0.1, 0.2, 0.3$) are included. From the results, we can intuitively see that the larger truncation order, the higher fidelity we achieve, which is in line with our theoretical analysis. And the phenomenon that we could still achieve a fidelity higher than 98% even under higher temperatures indicates that our hybrid algorithm has a powerful ability in preparing Gibbs states of certain many-body Hamiltonians.

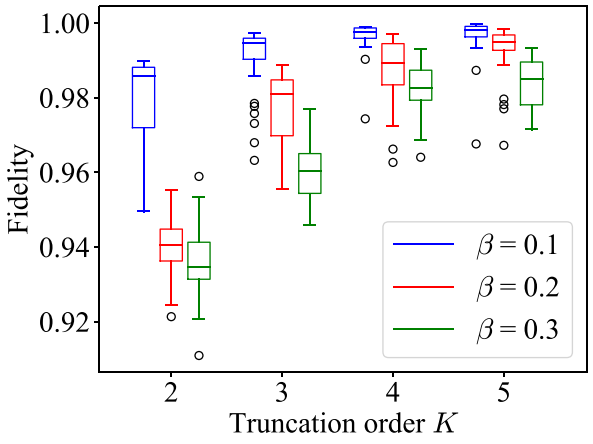

FIG. 9. Boxplot of the fidelity versus the truncation order K for different β for the *XY* spin-$\frac{1}{2}$ chain model. Here the ansatz is similar to Fig. 7 while $n_A = n_B = 3$. Each box consists of 30 runs with different parameter initializations.

IV. DISCUSSION

In this work, we provide variational quantum algorithms for quantum Gibbs state preparation with NISQ devices. We design loss functions to approximate the free energy of a given Hamiltonian by utilizing the truncated Taylor series of the von Neumann entropy. By minimizing the loss functions, the parameterized quantum circuits can be trained to learn the Gibbs state via variational algorithms since the Gibbs state minimizes free energy. In particular, we show that both the loss functions and their gradients can be evaluated on NISQ devices, thus allowing us to implement the hybrid quantum-classical optimization via either gradient-based or gradient-free optimization methods. Moreover, we show that our method could efficiently prepare the Gibbs states via analytical evidence and numerical experiments. We further show that our variational algorithms work efficiently for many-body models, including the Ising chain and spin chain models. In particular, we show that the preparation of the Ising Gibbs state can be done efficiently and accurately via shallow parameterized quantum circuits with only one parameter and one additional qubit. We expect that our results may shed light on quantum optimization, quantum simulation, and quantum machine learning in the NISQ era.

ACKNOWLEDGMENTS

We would like to thank Runyao Duan, Yuan Feng, and Sanjiang Li for helpful discussions. Y.W. and G.L. contributed equally to this work and acknowledge support from the Baidu-UTS AI Meets Quantum project. G.L. acknowledges financial support from the China Scholarship Council (No. 201806070139). This work is partly supported by the Australian Research Council (Grant No. DP180100691).

1: Input: choose the ansatz of unitary $U(\boldsymbol{\theta})$, tolerance ε, truncation order K, and initial parameters of $\boldsymbol{\theta}$;
2: Compute coefficients $C_0, C_1,..., C_K$ according to Eq. (7).
3: Prepare initial states $|00\rangle$ in registers AB and apply $U(\boldsymbol{\theta})$ to these states.
4: Measure and compute $\mathrm{tr}(H\rho_{B_1})$ and compute the loss function $L_1 = \mathrm{tr}(H\rho_{B_1})$;
5: Measure the overlap $\mathrm{tr}(\prod_{t_2\in\Sigma_2}\rho_{B_{t_2}})$ via Destructive Swap Test and compute the loss function $L_2 = -\beta^{-1}C_1\,\mathrm{tr}(\prod_{t_2\in\Sigma_2}\rho_{B_{t_2}})$;
6: Measure the overlap $\mathrm{tr}(\prod_{t_k\in\Sigma_k}\rho_{B_{t_k}})$ via higher order state overlap estimation and compute the loss function $L_k = -\beta^{-1}C_{k-1}\,\mathrm{tr}(\prod_{t_k\in\Sigma_k}\rho_{B_{t_k}})$ for each $k \in \{3, ..., K+1\}$.
7: Perform optimization of $\mathcal{F}_K(\boldsymbol{\theta}) = \sum_{k=1}^{K+1} L_k - \beta^{-1}C_0$ and update parameters of $\boldsymbol{\theta}$;
8: Repeat 3-7 until the loss function $\mathcal{F}_K(\boldsymbol{\theta})$ converges with tolerance ε;
9: Output: the state $\rho^{out} = \mathrm{tr}_A\, U(\boldsymbol{\theta})\,|00\rangle\langle 00|_{AB}\, U(\boldsymbol{\theta})^\dagger$.

Algorithm 2. Variational quantum Gibbs state preparation with truncation order K

APPENDIX A: VARIATIONAL ALGORITHM FOR GIBBS STATE PREPARATION WITH HIGHER-ORDER TRUNCATIONS

Here we present a variational algorithm for preparing the Gibbs state with K-truncated free energy. To illustrate our algorithm, we give some notation first. We let $A_{t_j}B_{t_j}$ denote the registers that store the states for estimating $\mathrm{tr}(\rho^t)$, where $t_j \in \Sigma_t$ and Σ_t includes all the indices of these registers.

APPENDIX B: TECHNICAL DETAILS

1. Proof of Lemma 2

First, we show the left inequality in Eq. (12). For an arbitrary density operator ρ, we have $\mathcal{F}_K(\rho) - \mathcal{F}(\rho) > 0$. To be specific,

$$\begin{aligned}\mathcal{F}_K(\rho) - \mathcal{F}(\rho) &= \beta^{-1}[S(\rho) - S_K(\rho)] \\ &= -\beta^{-1}\,\mathrm{tr}\left(\sum_{j=K+1}^{\infty}\frac{(-1)^{j+1}}{j}(\rho - I)^j\rho\right) > 0 \end{aligned} \tag{B1}$$

In Eq. (B1), we expand the von Neumann entropy in a Taylor series, i.e., $S(\rho) = -\mathrm{tr}[\sum_{j=1}^{\infty}(-1)^{j+1}/j\,(\rho - I)^j\rho]$, and the result holds immediately.

Second, the right inequality in Eq. (12) is a direct result of the definition of the truncated free energy $\mathcal{F}_K(\rho)$:

$$\begin{aligned}\mathcal{F}_K(\boldsymbol{\theta}_0) - \mathcal{F}(\rho_G) &= \mathcal{F}_K(\boldsymbol{\theta}_0) - \min_{\boldsymbol{\theta}}\mathcal{F}_K(\boldsymbol{\theta}) \\ &\quad + \min_{\boldsymbol{\theta}}\mathcal{F}_K(\boldsymbol{\theta}) - \mathcal{F}(\rho_G) \\ &\le \epsilon + \mathcal{F}_K(\rho_G) - \mathcal{F}(\rho_G) \\ &\le \epsilon + \beta^{-1}\delta_0. \end{aligned} \tag{B2}$$

In the first inequality we have used the fact that $\min_{\boldsymbol{\theta}}\mathcal{F}_K(\boldsymbol{\theta}) \le \mathcal{F}_K(\boldsymbol{\theta}_0) \le \min_{\boldsymbol{\theta}}\mathcal{F}_K(\boldsymbol{\theta}) + \epsilon$, and the second inequality is due to the truncation. Especially, we assume here that the PQC endows sufficient expressiveness to prepare the desired Gibbs state or a state very close to it, which allows $\min_{\boldsymbol{\theta}}\mathcal{F}_K(\boldsymbol{\theta}) \le \mathcal{F}_K(\rho_G)$.

2. Proof of Lemma 3

The proof proceeds by expanding the logarithm function in the entropy in a Taylor series. The upper bound of the difference between the entropy $S(\rho)$ and its truncated version $S_K(\rho)$ for density ρ is given as

$$\begin{aligned}\delta_0 &= |S(\rho) - S_K(\rho)| \\ &= \left|\mathrm{tr}\left(\sum_{k=K+1}^{\infty}\frac{(-1)^k}{k}(\rho - I)^k\rho\right)\right| \\ &= \left(\sum_{j:\lambda_j\ge\Delta} + \sum_{j:0<\lambda_j<\Delta}\right)\sum_{k=K+1}^{\infty}\frac{\lambda_j}{k}(1-\lambda_j)^k. \end{aligned} \tag{B3}$$

In Eq. (B3) we use the spectral decomposition of $\rho = \sum_{j=1}^{r}\lambda_j\,|\psi_j\rangle\langle\psi_j|$.

To give an upper bound on the truncation error δ_0, we give upper bounds on the two terms in Eq. (B3). First, we consider the term with eigenvalues larger than Δ.

$$\begin{aligned}&\sum_{j:\lambda_j\ge\Delta}\sum_{k=K+1}^{\infty}\frac{\lambda_j}{k}(1-\lambda_j)^k \\ &= \sum_{j:\lambda_j\ge\Delta}\sum_{k=K+1}^{\infty}\left[\frac{1}{k}(1-\lambda_j)^k - \frac{1}{k}(1-\lambda_j)^{k+1}\right] \qquad \text{(B4)} \\ &\le \sum_{j:\lambda_j\ge\Delta}\sum_{k=K+1}^{\infty}\frac{1}{k}(1-\lambda_j)^k \\ &\quad - \sum_{j:\lambda_j\ge\Delta}\sum_{k=K+1}^{\infty}\frac{1}{k+1}(1-\lambda_j)^{k+1} \qquad \text{(B5)} \\ &= \frac{1}{K+1}\sum_{j:\lambda_j\ge\Delta}(1-\lambda_j)^{K+1}. \end{aligned}$$

Equality (B4) is due to the substitution of λ_j with $1-(1-\lambda_j)$, and inequality (B5) follows by replacing $1/k$ with $1/(k+1)$ in the right summation of equality (B4).

Then we consider the term with nonzero eigenvalues less than Δ, i.e.,

$$\sum_{j:0<\lambda_j<\Delta}\lambda_j\sum_{k=K+1}^{\infty}\frac{1}{k}(1-\lambda_j)^k \le \sum_{j:0<\lambda_j<\Delta}-\lambda_j\ln(\lambda_j) \quad \text{(B6)}$$

$$\le \sum_{j:0<\lambda_j<\Delta}-\Delta\ln(\Delta), \quad \text{(B7)}$$

where inequality (B6) follows from replacing the series with $-\ln(\lambda_j)$, since the function $S(x)=-x\ln(x)=\sum_{l=1}^{\infty}(1/l)x(1-x)^l$, and inequality (B7) is due to the fact that $S(x)$ increases as x increases in the interval $(0,e^{-1})$.

In all, an upper bound on δ_0 can be given as

$$\begin{aligned}\delta_0 &\le \frac{1}{K+1}\sum_{j:\lambda_j\ge\Delta}(1-\lambda_j)^{K+1}+\sum_{j:0<\lambda_j<\Delta}-\Delta\ln(\Delta)\\ &\le r\times\left(\frac{r_0}{r}\frac{(1-\Delta)^{K+1}}{K+1}+\frac{r_1}{r}[-\Delta\ln(\Delta)]\right)\\ &\le r\times\max\left\{\frac{(1-\Delta)^{K+1}}{K+1},-\Delta\ln(\Delta)\right\},\end{aligned} \quad \text{(B8)}$$

where r_0 (r_1) denotes the number of nonzero eigenvalues larger (less) than Δ. As $-\Delta\ln(\Delta)<1/K+1(1-\Delta)^{K+1}$, the claim is proved.

3. Estimation of the higher-order gradients

Lemma 5: *Given a parameterized density operator $\rho(\boldsymbol{\theta})$, we have the equality*

$$\partial_{\theta_m}\operatorname{tr}(\rho(\boldsymbol{\theta})^3)=3\partial_{\theta_{m,1}}\operatorname{tr}[\rho_1(\boldsymbol{\theta})\otimes\rho_2(\boldsymbol{\theta})\otimes\rho_3(\boldsymbol{\theta})\times S_1S_2], \quad \text{(B9)}$$

where $\partial_{\theta_{m,1}}$ means that the derivative is computed with respective to θ_m of the state stored in the first register, $\rho_j(\boldsymbol{\theta})$ is the state stored in the j th register, $S_1=SWAP_{12}\otimes I_3$, $S_2=I_1\otimes SWAP_{23}$, and $SWAP_{ij}$ is the operator that swaps the state stored in the ith and j th registers.

Proof: To prove the claim, we need the following result, which we give a proof of later:

$$\begin{aligned}\operatorname{tr}(\rho_1\otimes\rho_2\otimes\rho_3\times S_1S_2)&=\overline{\operatorname{tr}(\rho_2\otimes\rho_1\otimes\rho_3\times S_1S_2)}\\ &=\overline{\operatorname{tr}(\rho_3\otimes\rho_2\otimes\rho_1\times S_1S_2)}.\end{aligned} \quad \text{(B10)}$$

Let $\rho_1(\boldsymbol{\theta})=\rho_2(\boldsymbol{\theta})=\rho_3(\boldsymbol{\theta})=\rho(\boldsymbol{\theta})$. Then the claim is proved as follows:

$$\begin{aligned}\frac{\partial}{\partial\theta_m}\operatorname{tr}[\rho(\boldsymbol{\theta})^3]&=\frac{\partial}{\partial\theta_m}\operatorname{tr}[\rho_1(\boldsymbol{\theta})\otimes\rho_2(\boldsymbol{\theta})\otimes\rho_3(\boldsymbol{\theta})\times S_1S_2]\\ &=\frac{\partial}{\partial\theta_{m,1}}\operatorname{tr}[\rho_1(\boldsymbol{\theta})\otimes\rho_2(\boldsymbol{\theta})\otimes\rho_3(\boldsymbol{\theta})\times S_1S_2]\\ &\quad+\frac{\partial}{\partial\theta_{m,2}}\operatorname{tr}[\rho_1(\boldsymbol{\theta})\otimes\rho_2(\boldsymbol{\theta})\otimes\rho_3(\boldsymbol{\theta})\times S_1S_2]\\ &\quad+\frac{\partial}{\partial\theta_{m,3}}\operatorname{tr}[\rho_1(\boldsymbol{\theta})\otimes\rho_2(\boldsymbol{\theta})\otimes\rho_3(\boldsymbol{\theta})\times S_1S_2]\end{aligned} \quad \text{(B11)}$$

$$\begin{aligned}&=\frac{\partial}{\partial\theta_{m,1}}\operatorname{tr}[\rho_1(\boldsymbol{\theta})\otimes\rho_2(\boldsymbol{\theta})\otimes\rho_3(\boldsymbol{\theta})\times S_1S_2]\\ &\quad+\frac{\partial}{\partial\theta_{m,2}}\operatorname{tr}[\rho_2(\boldsymbol{\theta})\otimes\rho_1(\boldsymbol{\theta})\otimes\rho_3(\boldsymbol{\theta})\times S_1S_2]\\ &\quad+\frac{\partial}{\partial\theta_{m,3}}\operatorname{tr}[\rho_3(\boldsymbol{\theta})\otimes\rho_2(\boldsymbol{\theta})\otimes\rho_1(\boldsymbol{\theta})\times S_1S_2]\\ &=3\frac{\partial}{\partial\theta_{m,1}}\operatorname{tr}[\rho_1(\boldsymbol{\theta})\otimes\rho_2(\boldsymbol{\theta})\otimes\rho_3(\boldsymbol{\theta})\times S_1S_2].\end{aligned} \quad \text{(B12)}$$

Here equality (B11) is the result of the chain rule, and we have used the relation in Eq. (B10) to derive equality (B12).

Now we prove the equalities in Eq. (B10). Let $\rho_1=\sum_j p_j|\phi_j\rangle\langle\phi_j|$, $\rho_2=\sum_l q_l|\psi_l\rangle\langle\psi_l|$, and $\rho_3=\sum_k r_k|\xi_k\rangle\langle\xi_k|$. We have the equalities

$$\operatorname{tr}(\rho_1\otimes\rho_2\otimes\rho_3\times S_1S_2)=\sum_{jlk}p_jq_lr_k\langle\psi_l|\phi_j\rangle\langle\xi_k|\psi_l\rangle\langle\phi_j|\xi_k\rangle, \quad \text{(B13)}$$

$$\operatorname{tr}(\rho_2\otimes\rho_1\otimes\rho_3\times S_1S_2)=\sum_{jlk}p_jq_lr_k\langle\phi_j|\psi_l\rangle\langle\xi_k|\phi_j\rangle\langle\psi_l|\xi_k\rangle, \quad \text{(B14)}$$

$$\operatorname{tr}(\rho_3\otimes\rho_2\otimes\rho_1\times S_1S_2)=\sum_{jlk}p_jq_lr_k\langle\psi_l|\xi_k\rangle\langle\phi_j|\psi_l\rangle\langle\xi_k|\phi_j\rangle. \quad \text{(B15)}$$

Comparing Eqs. (B13)–(B15), the equalities in Eq. (B10) are proved. ■

4. Supplementary discussion for optimization

To simplify the notation, let L_1 denote $\operatorname{tr}[H\rho(\boldsymbol{\theta})]$, L_2 denote $2\beta^{-1}\operatorname{tr}[\rho(\boldsymbol{\theta})^2]$, and L_3 denote $-\beta^{-1}/2\operatorname{tr}[\rho(\boldsymbol{\theta})^3]$. Using such notation, our loss function can be rewritten as $\mathcal{F}_2(\boldsymbol{\theta})=L_1+L_2+L_3-3\beta^{-1}/2$, and the gradient of

$\mathcal{F}_2(\boldsymbol{\theta})$ can be rewritten as

$$\nabla_{\boldsymbol{\theta}}\mathcal{F}_2(\boldsymbol{\theta}) = \nabla_{\boldsymbol{\theta}}L_1 + \nabla_{\boldsymbol{\theta}}L_2 + \nabla_{\boldsymbol{\theta}}L_3. \tag{B16}$$

Therefore, the gradient of $\mathcal{F}_K(\boldsymbol{\theta})$ can be estimated by computing the gradients of $L_j, j = 1,2,3$. Specifically, $\nabla_{\boldsymbol{\theta}}L_j$, $j = 2,3$, can be computed using the destructive swap test and higher-order state overlap estimation, respectively. As for $\nabla_{\boldsymbol{\theta}}L_1$, it can be estimated by measurement directly.

Next, we show that the gradients of the L_j can be computed by shifting the parameters $\boldsymbol{\theta}$ of the circuit. The partial derivatives of each L_j have the forms

$$\frac{\partial L_1}{\partial\theta_m} = \frac{\partial}{\partial\theta_m}\operatorname{tr}[U_N\cdots U_1|0\rangle\langle 0|U_1^\dagger\cdots U_N^\dagger \times (I\otimes H)], \tag{B17}$$

$$\frac{\partial L_2}{\partial\theta_m} = 2\beta^{-1}\frac{\partial}{\partial\theta_m}\operatorname{tr}[(U_N\cdots U_1|0\rangle\langle 0|U_1^\dagger\cdots U_N^\dagger)^{\otimes 2}\times W_1], \tag{B18}$$

$$\frac{\partial L_3}{\partial\theta_m} = -\frac{\beta^{-1}}{2}\frac{\partial}{\partial\theta_m}\operatorname{tr}[(U_N\cdots U_1|0\rangle\langle 0|U_1^\dagger\cdots U_N^\dagger)^{\otimes 3}\times W_2], \tag{B19}$$

where W_1 denotes the operator $\mathrm{SWAP}_{B_2B_3}\otimes I_{A_2A_3}$, W_2 denotes the operator $(\mathrm{SWAP}_{B_4B_5}\otimes I_{A_4A_5A_6B_6})\times(\mathrm{SWAP}_{B_5B_6}\otimes I_{A_4B_4A_5A_6})$, and the operator $\mathrm{SWAP}_{B_jB_l}$ is a swap operator acting on registers B_j and B_l.

To further simplify the notation, we absorb all gates before and after U_m into the density operator and measurement operator, respectively. To be more specific, let $\psi_{A_lB_l}$ denote the density operator $U_{m-1}\cdots U_1|00\rangle\langle 00|_{A_lB_l}U_1^\dagger\cdots U_{m-1}^\dagger$ in register A_lB_l for $l = 1,\ldots,6$. We define observable operators K, O, G as

$$K = U_{m+1}^\dagger\cdots U_N^\dagger(I_{A_1}\otimes H_{B_1})U_N\cdots U_{m+1}, \tag{B20}$$

$$O = (U_{m+1}^\dagger\cdots U_N^\dagger)^{\otimes 2}W_1(U_N\cdots U_{m+1})^{\otimes 2}, \tag{B21}$$

$$G = (U_{m+1}\cdots U_N^\dagger)^{\otimes 3}W_2(U_N\cdots U_{m+1})^{\otimes 3}. \tag{B22}$$

Then partial derivatives in Eqs. (B17)–(B19) can be rewritten as

$$\frac{\partial L_1}{\partial\theta_m} = \frac{\partial}{\partial\theta_m}\operatorname{tr}[U_m(\theta_m)\psi_{A_1B_1}U_m^\dagger(\theta_m)\times K], \tag{B23}$$

$$\frac{\partial L_2}{\partial\theta_m} = 2\beta^{-1}\frac{\partial}{\partial\theta_m}\operatorname{tr}[U_m\psi_{A_2B_2}U_m^\dagger(\theta_m) \otimes U_m\psi_{A_3B_3}U_m^\dagger(\theta_m)\times O], \tag{B24}$$

$$\frac{\partial L_3}{\partial\theta_m} = -\frac{\beta^{-1}}{2}\frac{\partial}{\partial\theta_m}\operatorname{tr}[U_m\psi_{A_4B_4}U_m^\dagger(\theta_m)\otimes U_m\psi_{A_5B_5}U_m^\dagger(\theta_m) \otimes U_m\psi_{A_6B_6}U_m^\dagger(\theta_m)\times G]. \tag{B25}$$

Now, we derive the analytical forms of the derivatives of each $L_j, j = 1,2,3$. Note that the trainable unitary $U(\boldsymbol{\theta})$ is a sequence of unitaries $U_m(\theta_m)$ and each unitary $U_m(\theta_m) = e^{-i\theta_m H_m/2}$. The partial derivative of $U(\boldsymbol{\theta})$ can be explicitly given as

$$\frac{\partial U(\boldsymbol{\theta})}{\partial\theta_m} = U_N(\theta_N)\cdots\frac{\partial U_m(\theta_m)}{\partial\theta_m}\cdots U_1(\theta_1), = -\frac{i}{2}U_N(\theta_N)\cdots H_mU_m\cdots U_1(\theta_1). \tag{B26}$$

Using the expression of $\partial_{\theta_m}U(\boldsymbol{\theta})$ in Eq. (B26) and some facts, including an identity $i[H_m,M] = U_m(-\pi/2)MU_m^\dagger(-\pi/2) - U_m(\pi/2)MU_m^\dagger(\pi/2)$, which holds for arbitrary matrix M, the symmetry of the operator O, and an equality $\partial_{\theta_m}\operatorname{tr}[\rho(\boldsymbol{\theta})^3] = 3\partial_{\theta_{m1}}\operatorname{tr}[\rho_1(\boldsymbol{\theta})\otimes\rho_2(\boldsymbol{\theta})\otimes\rho_3(\boldsymbol{\theta})\times S_1S_2]$ (cf. Lemma 5), where $S_1 = \mathrm{SWAP}_{12}\otimes I_3$ and $S_2 = I_1\otimes\mathrm{SWAP}_{23}$, the gradients of each L_j can be estimated using the formulae

$$\frac{\partial L_1}{\partial\theta_m} = \frac{1}{2}(\langle K\rangle_{\theta_m+\pi/2} - \langle K\rangle_{\theta_m-\pi/2}), \tag{B27}$$

$$\frac{\partial L_2}{\partial\theta_m} = 2\beta^{-1}(\langle O\rangle_{\theta_m+\pi/2,\theta_m} - \langle O\rangle_{\theta_m-\pi/2,\theta_m}), \tag{B28}$$

$$\frac{\partial L_3}{\partial\theta_m} = -\frac{3\beta^{-1}}{4}(\langle G\rangle_{\theta_m+\pi/2,\theta_m,\theta_m} - \langle G\rangle_{\theta_m-\pi/2,\theta_m,\theta_m}), \tag{B29}$$

where the notation $\langle X\rangle_{a,b}$ is defined as

$$\langle K\rangle_{\theta_\alpha} = \operatorname{tr}(U_\alpha\psi_{A_1B_1}U_\alpha^\dagger\times K), \tag{B30}$$

$$\langle O\rangle_{\theta_\alpha,\theta_\beta} = \operatorname{tr}(U_\alpha\psi_{A_2B_2}U_\alpha^\dagger\otimes U_\beta\psi_{A_3B_3}U_\beta^\dagger\times O), \tag{B31}$$

$$\langle G\rangle_{\theta_\alpha,\theta_\beta,\theta_\gamma} = \operatorname{tr}(U_\alpha\psi_{A_4B_4}U_\alpha^\dagger\otimes U_\beta\psi_{A_5B_5}U_\beta^\dagger \otimes U_\gamma\psi_{A_6B_6}U_\gamma^\dagger\times G). \tag{B32}$$

5. Proof of Proposition 1

This claim can be directly derived by computing the global minimum of both loss functions $\mathcal{F}$ and $\mathcal{F}_2$ using the ansatz in Fig. 4(b). Assuming that $n_A = 1$, $n_B = n$ and denoting the output state as $|\psi\rangle_{AB}$, we can easily obtain the state ρ_B as

$$\rho_B(\theta) = \operatorname{tr}_A(|\psi\rangle\langle\psi|_{AB}) = \cos^2(\theta/2)|0^n\rangle\langle 0^n|_B + \sin^2(\theta/2)|1^n\rangle\langle 1^n|_B. \tag{B33}$$

To compute the derivatives of $\mathcal{F}(\theta)$ and $\mathcal{F}_2(\theta)$, we first present their explicit expressions:

$$\mathcal{F}(\theta) = \operatorname{tr}[H_B\rho_B(\theta)] - \beta^{-1}S[\rho_B(\theta)] = \lambda_0 a + \lambda_1 b + \beta^{-1}[a\ln(a) + b\ln(b)], \tag{B34}$$

$$\begin{aligned}\mathcal{F}_2(\theta) &= \mathrm{tr}[H_B\rho_B(\theta)] \\ &\quad + \beta^{-1}\left[2\,\mathrm{tr}[\rho_B(\theta)^2] - \frac{1}{2}\,\mathrm{tr}[\rho_B(\theta)^3] - \frac{3}{2}\right] \\ &= \lambda_0 a + \lambda_1 b + \beta^{-1}\left[2a^2 + 2b^2 - \frac{a^3+b^3}{2} - \frac{3}{2}\right].\end{aligned} \tag{B35}$$

Here we have denoted $\cos^2(\theta/2)$ by a and $\sin^2(\theta/2)$ by b, and λ_0 and λ_1 are the eigenvalues of H associated with eigenvectors $|0^n\rangle$ and $|1^n\rangle$, respectively.

Actually, in the Ising chain model, λ_0 and λ_1 are equal (cf. Lemma 6). Thus, derivatives of $\mathcal{F}[\rho_B(\theta)]$ and $\mathcal{F}_2[\rho_B(\theta)]$ with respect to θ have the forms

$$\partial_\theta \mathcal{F}(\theta) = \frac{\beta^{-1}}{2}\sin(\theta)[\ln(b) - \ln(a)], \tag{B36}$$

$$\partial_\theta \mathcal{F}_2(\theta) = \frac{5\beta^{-1}}{2}\sin(\theta)(b-a). \tag{B37}$$

From Eqs. (B36) and (B37), the global minimums of $\mathcal{F}$ and $\mathcal{F}_2$ are

$$\theta = \frac{\pi}{2} + k\pi \quad \text{for all } k \in \mathbb{Z}. \tag{B38}$$

The fidelity between $\rho_B(\pi/2)$ and ρ_G could be derived from Proposition 2 and Lemma 6, where if we set $N = 2^5$, $\Delta = 4$, and $\beta = 1.25$ then we get $F[\rho_B(\pi/2), \rho_G] \geq 95.3\%$. Hence, we could achieve a fidelity higher than 95%, provided that $\beta \geq 1.25$.

6. Proof of Proposition 2

Proof: To prove this result, we assume that the eigenvalues, associated with the eigenvectors $|0\rangle, |1\rangle, \ldots, |N-1\rangle$, for the Hamiltonian H are denoted by $\lambda_0, \lambda_1, \ldots, \lambda_{N-1}$. Specifically, eigenvalues λ_0 and λ_{N-1} are associated with eigenvectors $|0^n\rangle$ and $|1^n\rangle$, respectively. A key feature of the Ising model is that $\lambda_0 = \lambda_{N-1}$, which are minimum among all eigenvalues, implying that $\lambda_j - \lambda_0 \geq \Delta$ for $j \neq 0, N-1$, where Δ denotes the spectral gap of the Hamiltonian H_B.

Let $\hat{\lambda}_j$ denote the eigenvalues of the Gibbs state. Then, according to the definition of the Gibbs state, $\hat{\lambda}_j$ has the form

$$\hat{\lambda}_j = \frac{e^{-\beta\lambda_j}}{Z}, \tag{B39}$$

where $Z = \sum_{l=0}^{N-1} e^{-\beta\lambda_l}$.

Next, we derive bounds on eigenvalues $\hat{\lambda}_0$ and $\hat{\lambda}_{N-1}$. Note that, in the Ising model, eigenvalues λ_0 and λ_{N-1} are equal; then the associated eigenvalues $\hat{\lambda}_0 = \hat{\lambda}_{N-1}$, and they have the following explicit forms:

$$\begin{aligned}\hat{\lambda}_0 &= \hat{\lambda}_{N-1} \\ &= \frac{e^{-\beta\lambda_0}}{Z} \\ &= \frac{1}{2 + \sum_{j\neq 0,N-1} e^{\beta(\lambda_0 - \lambda_j)}} \\ &\geq \frac{1}{2 + (N-2)e^{-\beta\Delta}}.\end{aligned} \tag{B40}$$

Recall that the output state of our algorithm is $\rho_B(\pi/2)$ in Proposition 1. The inequality in Eq. (23) is immediately acquired by calculating the fidelity $F[\rho_B(\pi/2), \rho_G]$:

$$\begin{aligned}F(\rho_B(\pi/2), \rho_G) &= \mathrm{tr}\sqrt{\rho_B^{1/2}(\pi/2)\rho_G\rho_B^{1/2}(\pi/2)} \\ &= \mathrm{tr}\sqrt{1/\sqrt{2}\times\hat{\lambda}_0\times 1/\sqrt{2}|0^n\rangle\langle 0^n| + 1/\sqrt{2}\times\hat{\lambda}_{N-1}\times 1/\sqrt{2}|1^n\rangle\langle 1^n|} \\ &= \sqrt{2\hat{\lambda}_0} \\ &\geq \frac{1}{\sqrt{1 + (N/2-1)e^{-\beta\Delta}}}.\end{aligned} \tag{B41}$$

This completes the proof. ■

The following lemma states some facts about the Ising model, which are helpful for the above proofs.

Lemma 6: *Given the Ising model Hamiltonian in Eq. (21), the eigenvalues λ_0 and λ_{N-1}, associated with eigenvectors $|0^{n_B}\rangle$ and $|1^{n_B}\rangle$, are equal, i.e., $\lambda_0 = \lambda_{N-1} = -L$. In particular, the spectral gap is exactly 4 for all $n_B \geq 2$.*

Proof: To prove that the eigenvalues of $|0^{n_B}\rangle$ and $|1^{n_B}\rangle$ are equal, we compute the corresponding eigenvalues of each term $Z_{B,i}Z_{B,i+1}$. Note that, for all $i = 1, \ldots, L$,

$$Z_{B,i}Z_{B,i+1}\,|0^{n_B}\rangle = |0^{n_B}\rangle\,, \tag{B42}$$

$$Z_{B,i}Z_{B,i+1}\,|1^{n_B}\rangle = |1^{n_B}\rangle\,. \tag{B43}$$

Hence, in the Ising model, the eigenvalues of $|0^{n_B}\rangle$ and $|1^{n_B}\rangle$ are $-L$.

As for the rest of the eigenvectors, $|j\rangle$, $j \neq 0, N-1$, the eigenvalues of $Z_{B,i}Z_{B,i+1}$ are given as

$$Z_{B,i}Z_{B,i+1}\,|j\rangle = (-1)^{k_i+k_{i+1}}\,|j\rangle\,, \tag{B44}$$

where k_i and k_{i+1} are the bits in the ith and $(i+1)$th positions of $|j\rangle$. In particular, in the Ising model, the eigenvalue of $|j\rangle$ is represented as $-\sum_{i=1}^{L}(-1)^{k_{B,i}+k_{B,i+1}}$. To be specific,

$$H_B\,|j\rangle = -\sum_{i=1}^{L}(-1)^{k_i+k_{i+1}}\,|j\rangle\,. \tag{B45}$$

Overall, the eigenvalues of $|j\rangle$ are larger than $-L$, which implies that the eigenvalues of $|0^{n_B}\rangle$ and $|1^{n_B}\rangle$ are minimum.

Now we show that the spectral gap of the Ising model with more than two qubits is 4. The minimum eigenvalue of H_B is $-L$ means that $k_{B,i} + k_{B,i+1} = 0/2$ for all i, and hence the ground states are $|0^{n_B}\rangle$ and $|1^{n_B}\rangle$. If we flip one qubit of the eigenvector $|j\rangle$, then two terms like $(-1)^{k_{B,i}+k_{B,i+1}}$ of its eigenvalues will change by 2. If we flip more qubits, then more terms will change. Note that the eigenvectors with an eigenvalue larger than $-L$ will differ from those with minimum eigenvalue at least one qubit, resulting in at least two term changes. Then, the overall difference between the minimum and second minimum eigenvalues is at least 4. Clearly, a difference of 4 can be obtained, and so the spectral gap is 4. ■

[1] Andrew M. Childs, Dmitri Maslov, Yunseong Nam, Neil J. Ross, and Yuan Su, Toward the first quantum simulation with quantum speedup, Proceedings of the National Academy of Sciences **115**, 9456 (2018).

[2] Mária Kieferová and Nathana Wiebe, Tomography and generative training with quantum boltzmann machines, Phys. Rev. A **96**, 062327 (2017).

[3] Jacob Biamonte, Peter Wittek, Nicola Pancotti, Patrick Rebentrost, Nathan Wiebe, and Seth Lloyd, Quantum machine learning, Nature **549**, 195 (2017).

[4] Rolando D. Somma, Sergio Boixo, Howard Barnum, and Emanuel Knill, Quantum Simulations of Classical Annealing Processes, Phys. Rev. Lett. **101**, 130504 (2008).

[5] Fernando G. S. L. Brandao and Krysta M. Svore, in *2017 IEEE 58th Annual Symposium on Foundations of Computer Science (FOCS)* (IEEE, 2017), p. 415.

[6] Mária Kieferová and Nathan Wiebe, Tomography and generative training with quantum boltzmann machines, Phys. Rev. A **96**, 062327 (2017).

[7] John Watrous, in *Computational Complexity*, Vol. 978146 1418 (Springer New York, New York, NY, 2012), p. 2361.

[8] Dorit Aharonov, Itai Arad, and Thomas Vidick, Guest column: The quantum pcp conjecture, Acm Sigact News **44**, 47 (2013).

[9] Barbara M. Terhal and David P. DiVincenzo, Problem of equilibration and the computation of correlation functions on a quantum computer, Phys. Rev. A **61**, 022301 (2000).

[10] David Poulin and Pawel Wocjan, Sampling from the Thermal Quantum Gibbs State and Evaluating Partition Functions with a Quantum Computer, Phys. Rev. Lett. **103**, 220502 (2009).

[11] Kristan Temme, Tobias J. Osborne, Karl G. Vollbrecht, David Poulin, and Frank Verstraete, Quantum metropolis sampling, Nature **471**, 87 (2011).

[12] Michael J. Kastoryano and Fernando G.S.L. Brandao, Quantum gibbs samplers: The commuting case, Commun. Math. Phys. **344**, 915 (2016).

[13] Fernando G.S.L. Brandão and Michael J. Kastoryano, Finite correlation length implies efficient preparation of quantum thermal states, Commun. Math. Phys. **365**, 1 (2019).

[14] Nathan Wiebe, Ashish Kapoor, and Krysta M. Svore, Quantum deep learning, Quantum Inf. Comput. **16**, 541 (2016).

[15] M.-H. Yung and Alán Aspuru-Guzik, A quantum-quantum metropolis algorithm, Proceedings of the National Academy of Sciences **109**, 754 (2012).

[16] David B. Kaplan, Natalie Klco, and Alessandro Roggero, Ground States via Spectral Combing on a Quantum Computer, (2017) ArXiv:1709.08250.

[17] Arnau Riera, Christian Gogolin, and Jens Eisert, Thermalization in Nature and on a Quantum Computer, Phys. Rev. Lett. **108**, 080402 (2012).

[18] Mario Motta, Chong Sun, Adrian Teck Keng Tan, Matthew J. O'Rourke, Erika Ye, Austin J. Minnich, Fernando G. S. L. Brandão, and Garnet Kin-Lic Chan, Determining eigenstates and thermal states on a quantum computer using quantum imaginary time evolution, Nat. Phys. **16**, 205 (2020).

[19] Ersen Bilgin and Sergio Boixo, Preparing Thermal States of Quantum Systems by Dimension Reduction, Phys. Rev. Lett. **105**, 170405 (2010).

[20] Joran Van Apeldoorn, András Gilyén, Sander Gribling, and Ronald de Wolf, Quantum sdp-solvers: Better upper and lower bounds, Quantum **4**, 230 (2020).

[21] Jarrod R. McClean, Jonathan Romero, Ryan Babbush, and Alán Aspuru-Guzik, The theory of variational hybrid quantum-classical algorithms, New J. Phys. **18**, 023023 (2016).

[22] Xiaosi Xu, Jinzhao Sun, Suguru Endo, Ying Li, Simon C. Benjamin, and Xiao Yuan, Variational algorithms for linear algebra, Science Bulletin **66**, 2181 (2021).

[23] Carlos Bravo-Prieto, Ryan LaRose, Marco Cerezo, Yigit Subasi, Lukasz Cincio, and Patrick Coles, Variational

quantum linear solver: A hybrid algorithm for linear systems, Bulletin of the American Physical Society **65**, ArXiv:1909.05820 (2019).

[24] Hsin-Yuan Huang, Kishor Bharti, and Patrick Rebentrost, Near-term quantum algorithms for linear systems of equations, arXiv preprint ArXiv:1909.07344 (2019).

[25] Ryan LaRose, Arkin Tikku, Étude O'Neel-Judy, Lukasz Cincio, and Patrick J. Coles, Variational quantum state diagonalization, npj Quantum Inf. **5**, 1 (2019).

[26] M. Cerezo, Kunal Sharma, Andrew Arrasmith, and Patrick J. Coles, Variational Quantum State Eigensolver, 1–14 (2020), ArXiv:2004.01372.

[27] Youle Wang, Guangxi Li, and Xin Wang, A Hybrid Quantum-Classical Hamiltonian Learning Algorithm, ArXiv:2103.01061.

[28] Alberto Peruzzo, Jarrod McClean, Peter Shadbolt, Man-Hong Yung, Xiao-Qi Zhou, Peter J. Love, Alán Aspuru-Guzik, and Jeremy L. O'brien, A variational eigenvalue solver on a photonic quantum processor, Nat. Commun. **5**, 4213 (2014).

[29] Ken M. Nakanishi, Kosuke Mitarai, and Keisuke Fujii, Subspace-search variational quantum eigensolver for excited states, Phys. Rev. Res. **1**, 033062 (2019).

[30] Xin Wang, Zhixin Song, and Youle Wang, Variational quantum singular value decomposition, Quantum **5**, 483 (2021).

[31] Kunal Sharma, Sumeet Khatri, M. Cerezo, and Patrick J. Coles, Noise resilience of variational quantum compiling, New J. Phys. **22**, 043006 (2020).

[32] G. Li, Z. Song, and X. Wang, VSQL: Variational shadow quantum learning for classification, (2021).

[33] Ranyiliu Chen, Zhixin Song, Xuanqiang Zhao, and Xin Wang, Variational Quantum Algorithms for Trace Distance and Fidelity Estimation, ArXiv:2012.05768, 1 (2020).

[34] Rajibul Islam, Ruichao Ma, Philipp M. Preiss, M. Eric Tai, Alexander Lukin, Matthew Rispoli, and Markus Greiner, Measuring entanglement entropy in a quantum many-body system, (2015).

[35] Guillaume Verdon, Jacob Marks, Sasha Nanda, Stefan Leichenauer, and Jack Hidary, Quantum hamiltonian-based models and the variational quantum thermalizer algorithm, Bulletin of the American Physical Society **65**, 00 (2020).

[36] Jingxiang Wu and Timothy H. Hsieh, Variational Thermal Quantum Simulation via Thermofield Double States, Phys. Rev. Lett. **123**, 220502 (2019).

[37] John Martyn and Brian Swingle, Product spectrum ansatz and the simplicity of thermal states, Phys. Rev. A **100**, 032107 (2019).

[38] Sam McArdle, Tyson Jones, Suguru Endo, Ying Li, Simon C. Benjamin, and Xiao Yuan, Variational ansatz-based quantum simulation of imaginary time evolution, npj Quantum Inf. **5**, 1 (2019).

[39] Xiao Yuan, Suguru Endo, Qi Zhao, Ying Li, and Simon C. Benjamin, Theory of variational quantum simulation, Quantum **3**, 191 (2019).

[40] Anirban N. Chowdhury, Guang Hao Low, and Nathan Wiebe, A Variational Quantum Algorithm for Preparing Quantum Gibbs States, ArXiv:2002.00055.

[41] Frederick Reif, *Fundamentals of Statistical and Thermal Physics* (Waveland Press, Long Grove, Ill., 2009), p. 651.

[42] Alexandru Gheorghiu and Matty J. Hoban, Estimating the entropy of shallow circuit outputs is hard, ArXiv:2002.12814.

[43] Sathyawageeswar Subramanian and Min-Hsiu Hsieh, Quantum algorithm for estimating α-renyi entropies of quantum states, Phys. Rev. A **104**, 022428 (2021).

[44] Tongyang Li and Xiaodi Wu, Quantum query complexity of entropy estimation, IEEE Transactions on Information Theory **65**, 2899 (2019).

[45] Gilles Brassard, Peter Høyer, Michele Mosca, and Alain Tapp, in *Contemporary Mathematics*, Vol. 305 (Providence, RI; American Mathematical Society; 1999, 2002), p. 53.

[46] Guang Hao Low and Isaac L. Chuang, Hamiltonian simulation by qubitization, Quantum **3**, 163 (2019).

[47] Marcello Benedetti, Erika Lloyd, Stefan Sack, and Mattia Fiorentini, Parameterized quantum circuits as machine learning models, Quantum Science and Technology, 1–18 (2019), ArXiv:1906.07682.

[48] Gian Giacomo Guerreschi and Mikhail Smelyanskiy, Practical optimization for hybrid quantum-classical algorithms, arXiv preprint ArXiv:1701.01450, 1 (2017).

[49] Guillaume Verdon, Michael Broughton, and Jacob Biamonte, A quantum algorithm to train neural networks using low-depth circuits, ArXiv:1712.05304 (2017).

[50] Dave Wecker, Matthew B. Hastings, and Matthias Troyer, Training a quantum optimizer, Phys. Rev. A **94**, 022309 (2016).

[51] Zhihui Wang, Stuart Hadfield, Zhang Jiang, and Eleanor G. Rieffel, Quantum approximate optimization algorithm for maxCut: A fermionic view, Phys. Rev. A **97**, 022304 (2018).

[52] Diederik P. Kingma and Jimmy Ba, Adam: A method for stochastic optimization, arXiv preprint ArXiv:1412.6980 (2014).

[53] Harry Buhrman, Richard Cleve, John Watrous, and Ronald de Wolf, Quantum Fingerprinting, Phys. Rev. Lett. **87**, 167902 (2001).

[54] Daniel Gottesman and Isaac Chuang, Quantum Digital Signatures, (2001), ArXiv:quant-ph/0105032.

[55] Artur K. Ekert, Carolina Moura Alves, Daniel K. L. Oi, Michał Horodecki, Paweł Horodecki, and Leong Chuan Kwek, Direct Estimations of Linear and Nonlinear Functionals of a Quantum State, Phys. Rev. Lett. **88**, 217901 (2002).

[56] Juan Carlos Garcia-Escartin and Pedro Chamorro-Posada, Swap test and hong-ou-Mandel effect are equivalent, Phys. Rev. A **87**, 052330 (2013).

[57] Raj B. Patel, Joseph Ho, Franck Ferreyrol, Timothy C. Ralph, and Geoff J. Pryde, A quantum fredkin gate, Sci. Adv. **2**, e1501531 (2016).

[58] Norbert M. Linke, Sonika Johri, Caroline Figgatt, Kevin A. Landsman, Anne Y. Matsuura, and Christopher Monroe, Measuring the Rényi entropy of a two-site fermi-hubbard model on a trapped ion quantum computer, Phys. Rev. A **98**, 052334 (2018).

[59] Lukasz Cincio, Yigit Subasi, Andrew T. Sornborger, and Patrick J. Coles, Learning the quantum algorithm for state overlap, New J. Phys. **20**, 113022 (2018).

[60] Yigit Subasi, Lukasz Cincio, and Patrick J. Coles, Entanglement spectroscopy with a depth-two quantum circuit, J. Phys. A: Math. Theor. **52**, 044001 (2019).

[61] Justin Yirka and Yiğit Subaşı, Qubit-efficient entanglement spectroscopy using qubit resets, Quantum **5**, 535 (2021).
[62] Eric Carlen, Trace inequalities and quantum entropy: An introductory course, Entropy and the Quantum **529**, 73 (2010).
[63] Kosuke Mitarai, Makoto Negoro, Masahiro Kitagawa, and Keisuke Fujii, Quantum circuit learning, Phys. Rev. A **98**, 032309 (2018).
[64] Maria Schuld, Ville Bergholm, Christian Gogolin, Josh Izaac, and Nathan Killoran, Evaluating analytic gradients on quantum hardware, Phys. Rev. A **99**, 032331 (2019).
[65] Mateusz Ostaszewski, Edward Grant, and Marcello Benedetti, Quantum circuit structure learning, 1–11 (2019), ArXiv:1905.09692.
[66] Edward Farhi and Hartmut Neven, Classification with Quantum Neural Networks on Near Term Processors, 1–21 (2018), ArXiv:1802.06002.